SHELL AND TUBE HEAT EXCHANGER NUMERICAL SIMULATION EMPLOYING HELICAL BAFFLES AND SELF-SUPPORT FINNED COMBINATION

by

Jinxing WU*, Chenxu WANG, Shengguang LU, and Jiawen LI

School of Mechanical and Power Engineering, Zhengzhou University, Zhengzhou, China

Original scientific paper
https://doi.org/10.2298/TSCI250321105W

To overcome the defect of reduced comprehensive performance caused by the installation of central tube in helical baffle heat exchanger (STHX-HBCT), a novel heat exchanger employing helical baffles and self-support finned tube (STHX-HBST) was proposed in this study. Numerical simulations were conducted to compare the thermal and hydraulic performance of shell and tube heat exchanger with segmental baffle (STHX-SG), STHX-HBCT, the helical baffle heat exchanger (STHX-HB). The results show that STHX-HBST has superior comprehensive performance, efficiency evaluation coefficient, compared to the other three types STHX. The effect of the helix angle of fins on the heat transfer performance and pressure drop of the heat exchanger was analyzed, the best comprehensive performance was achieved when the fin helix angle was 50°. This study provides a new solution for the structural improvement of helical baffle heat exchangers.

Key words: *shell and tube heat exchanger with helical baffle, self-support fin, comprehensive performance, numerical simulation*

Introduction

Due to the advantages of simple structure, mature manufacturing process, and strong applicability, STHX-SG are extensively applied in industrial fields [1]: chemical engineering, metallurgy, petroleum, and waste heat recovery. The segmental baffle, a key component of the STHX-SG, not only provides structural support for the tube bundle but also directs fluid-flow in a zigzag pattern to enhance turbulence effects and improve heat transfer efficiency. However, this design suffers from several drawbacks, including flow dead zones, high pressure drops, increased susceptibility to tube bundle vibration [2]. It is necessary to develop novel and highly efficient shell side support structures to address these limitations of STHX-SG.

The STHX-HB was proposed by Lutcha and Nemcansky [3]. This design employed a series of fan shaped baffles connected end to end in the shell side, generating pseudo spiral flow in the shell that effectively eliminated flow dead zones and enhanced heat transfer efficiency. Extensive research [4, 5] had demonstrated that, due to the scouring effect of secondary flow on boundary-layers generated by spiral flow in shell side, STHX-HB exhibited significantly superior comprehensive performance compared to STHX-SG under identical configurations. These advantages made STHX-HB be extensively studied [6, 7]. The helix angle was a crucial parameter that affected the performance of STHX-HB, and its optimal value had been widely investigated. Zhang *et al.* [8] conducted simulation study on quadrant STHX-QHB with helix angle ranging

* Corresponding author, e-mail: 17803865040@163.com

from 10°-30°, the performance is optimal when the helix angle is 30°. Lei *et al.* [9] made comprehensive comparison of the helix angles between 15° and 50°, concluding that the comprehensive performance, $h/\Delta p$, is highest at helix angle of 45°. Xiao *et al.* [10] studied the effect of helix angle on STHX-HB with different Prandtl numbers, revealing that for high viscosity fluids, the large helix angle weakened the flow diversion effect of the baffles, leading to reduced overall performance. Dong *et al.* [11] analyzed four different configurations of STHX-HB, showing that the circumferential overlapping structure suppresses fluid short circuit while enhancing the strength of secondary vortex in the shell side.

A variety of studies have explored the integration of STHX-HB with high efficiency heat exchange tubes to achieve better thermal performance. Du *et al.* [12] proposed an STHX-HB with elliptical tube at varying arrangement angles. The results showed that, comprehensive performance was improved by 50% compared with circle tube. Zhang *et al.* [13] employed 3-D petal-shaped finned tubes with diverse geometric parameters to enhance the heat transfer of STHX-HB. The results demonstrate that both the heat transfer coefficient and pressure drop of the 3-D finned tubes increased relative to smooth tubes, while the enhancement in heat flux significantly outweighed the rise in pressure drop. Gu *et al.* [14] proposed a STHX-HB equipped with elliptical twisted tubes, applying the field synergy principle to demonstrate a 16%-22.5% improvement in overall performance.

The triangular region formed between two adjacent baffles in discontinuous STHX-HB, which leading to fluid short circuit in the shell side and degrading heat transfer performance. To block the triangular region and prevent heat transfer capacity reduction in STHX-HB, researchers have proposed several improved baffle structures [15]. While the use of continuous helical baffle can avoid the influence of triangular leakage zones, complex machining and perforation requirements pose significant manufacturing challenges for STHX-HB [16]. In practical applications, a central tube [17] must be arranged, though it occupies the space of the shell side in the heat exchanger and reduces the number of heat exchange tubes. Wang *et al.* [18] proposed combined multiple shell pass shell and tube heat exchanger (STHX-CSTSP). The results showed that the leakage flow reducing heat transfer formed between the annulus separator and shell. Under the same thermal load, the total pressure drop of STHX-CSTSP was lower than that of STHX-SG. Yang *et al.* [19] introduced combined single shell pass shell and tube heat exchanger (STHX-CSSP), where fluid mixing occurred between the inner and outer layers of the helical baffle and formed complex flow field. The comprehensive performance, $h/\Delta p$, of STHX-CSSP surpassed both STHX-HB and STHX-SG. Uosofvand *et al.* [20] proposed heat exchanger with hybrid segmental and helical baffles (STHX-HSHB), generating a combined flow pattern with zigzag and helical characteristics on the shell side, efficiency evaluation coefficient (EEC) of STHX-HSHB was 58.2% higher than that of STHX-HB.

To further reduce the resistance of STHX and improve comprehensive performance, a novel heat exchanger with STHX-HBST was proposed in this study. The support structure of the heat exchanger consists of outer layer of helical baffle and inner layer of fins wound around the tubes, with no sleeve between baffle and fins. The height of the self-supporting fins equals the distance between the heat exchange tubes, forming point supports between the fins and the tubes. The self-supporting fins guide the fluid to form localized helical flow around the tubes, generating vortices and secondary flows [21]. Replacing the central tube with self-supporting finned tubes can fully utilizes the heat transfer space and enhances the heat exchanger's compactness. Moreover, the complex flow field generated on the shell side can enhances fluid mixing and further reduces the pressure drop.

Model foundation

Geometric model generation

As shown in fig. 1, the metal thin sheets are rolled into fins, which are wound around the inner heat exchange tubes close to the center of shell. The height of the fins equals the spacing between the heat exchange tubes, enabling self-support between the tubes through effect of the fins. The fins guide the fluid to form helical flow around the tubes while also acting as turbulence promoters. The outer tube bundle relies on helical baffle as the supporting structure. In addition, models of STHX-HB, STHX-HBCT, STHX-SG are established. To further evaluate the thermohydraulic performance of STHX-HBST and determine which support structure offers more advantages, the flow field patterns and comprehensive performance of the four heat exchangers are compared. Given the limitations of the numerical simulation calculation capability, the detailed geometric parameters of four heat exchangers are listed in tab. 1. The four types of heat exchangers share the same shell diameter, tube bundle arrangement, and effective tube length. Each heat exchanger utilizes nineteen heat exchange tubes, with the central tube diameter of STHX-HBCT set at 19% of the shell diameter. The pitch of the helical baffle is equal to the space of the segmental baffle, and pitch of the fins is set to 30 mm. To simplify the model and facilitate calculations, the following assumptions are made:

– The thickness of the baffles and the heat exchange tube walls is neglected.
– The gaps between the baffles and tubes are ignored.
– The wall surface of the heat exchange tubes is set to a constant wall temperature.
– There is no heat exchange between the heat exchanger and the surrounding environment.
– A small gap is introduced between the fins and the tube wall to simplify the calculation.

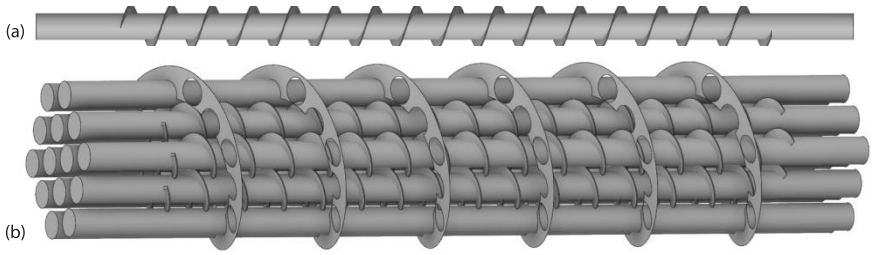

Figure 1. Physical model of STHX-HBST; (a) finned tube and (b) structure of STHX-HBST

Table 1. Parameters of STHX

Geometric	Value
Diameter of shell	125 mm
Length of tube	600 mm
Tube number	18 for STHX-HBCT, 19 for others
Tube lay-out pattern	Triangle
Diameter of tube	19 mm
Baffle cut	24%
Diameter of central tube	24 mm
Baffle space/helix pitch of baffle	80 mm
Helix pitch of fin	30 mm
Diameter of pipe	40 mm

Simulation method

The governing equations describing the mass, energy, and momentum conservation [22]:
Continuity equation:

$$\frac{\partial(\rho u_j)}{\partial u_j} = 0 \tag{1}$$

Momentum equation:

$$\frac{\partial(u_i u_j)}{\partial(x_j)} = -\frac{\partial p}{\partial x_i} + \frac{\partial}{\partial x_j}\left[\mu\left(\frac{\partial u_i}{\partial x_j} + \frac{\partial u_j}{\partial x_i}\right)\right] \tag{2}$$

Energy equation:

$$\frac{\partial u_j T}{\partial x_j} = \frac{\partial}{\partial x_j}\left(\frac{\lambda}{\rho c_p}\frac{\partial T}{\partial x_j}\right) \tag{3}$$

Realizable k-ε model was adopted as computation model because it provides more accuracy in predicting complex flows involving large curvature, strong vortices, steep pressure gradients, and swirling motions, Ozden and Tari [23] studied a small heat exchanger using CFD simulation with different turbulence models. The results indicated that realizable k-ε model showed the highest agreement with the Bell method. The transport equation of realizable k-ε is:
Turbulent kinetic energy, k, equation:

$$\frac{\partial(\rho k)}{\partial t} + \frac{\partial(\rho k u_i)}{\partial x_i} = \frac{\partial}{\partial x_j}\left[\left(\mu + \frac{\mu_t}{\sigma_k}\right)\frac{\partial k}{\partial x_j} + G_k - \rho\varepsilon\right] \tag{4}$$

Turbulent energy dissipation, E, equation:

$$\frac{\partial(\rho k)}{\partial t} + \frac{\partial(\rho\varepsilon u_i)}{\partial x_i} = \frac{\partial}{\partial x_j}\left[\left(\mu + \frac{\mu_t}{\sigma_\varepsilon}\frac{\partial\varepsilon}{\partial x_j}\right)\right] + \rho C_1 E\varepsilon - \rho C_2 \frac{\varepsilon^2}{k + \sqrt{\nu\varepsilon}} \tag{5}$$

$$G_k = \rho\overline{u_i' u_j'}\frac{\partial u_j}{\partial x_i} \tag{6}$$

where G_k is the turbulent kinetic energy generated by the average velocity gradient, C– the model coefficients, $C_1 = 1.42$, $C_2 = 1.68$, σ_k and σ_ε – the turbulence Prandtl numbers, and Pr – the turbulent Prandtl number.

Boundary conditions

The CFD software FLUENT with pressure-based solver is used for numerical simulation. The governing equations are solved iteratively using the SIMPLE algorithm. Momentum, turbulence kinetic energy, and energy equations are all solved using a second order upwind scheme, and the convergence criteria are set with velocity residual of less than 10^{-5} and energy equation residual of less than 10^{-6}. For high Reynolds nimber turbulence model, the standard wall function method is applied near the wall. Water is adopted as the fluid medium for the shell side, and the thermal physical properties are listed in tab. 2. The boundary conditions of the simulation are shown in tab. 3.

Table 2. Property parameters of water (293 K)

Parameter	ρ [kgm^{-3}]	C_p [Jkg^{-1}K^{-1}]	λ [Wm^{-1}K^{-1}]	$\mu \cdot 10^3$ [Pa·s]
Value	998.2	4182	0.613	1.003

Table 3. Boundary condition in simulation

	Type of boundary	Working fluid	Temperature	Mass-flow rate
Shell inlet	Velocity inlet	Cold water	293 K	0.5-4.5 kg/s
Shell outlet	Pressure outlet	Cold water	–	–
Tube wall	Constant wall temperature	–	353 K	–
Solid wall	No slip adiabatic walls	–	–	–

Grid independence test

The 3-D models were constructed in SCDM, considering the complex characteristics of fluid domain in shell side, polyhedral grids were generated in FLUENT Meshing to reduce the number of elements and improve computational efficiency. Figure 2 shows the mesh of the STHX. The grid independence test was conducted for STHX to ensure the accuracy of calculation. Three different mesh systems were established by modifying the local mesh size. For STHX-HBST 4993653, 8442668, and 10529687 mesh elements were generated. For STHX-HBCT, 2801203, 4593426, and 6734906 mesh elements were generated. For STHX-HB, 2845623, 4656125, and 6944993 mesh elements were generated. For STHX-SG, 2773944, 3780226 and 4570012 mesh elements were generated. As shown in fig. 3, when the number of grids increased from 8442668-10639687, the variations in the convective heat transfer coefficient, h, and pressure drop, Δp, of STHX-HBST were less than 1%. Considering solution accuracy and computation time, the scheme with 8.44 million was determined for the simulation. For the other three types of heat exchangers, the selected mesh counts were 4593426, 4656125, and 3780226, respectively.

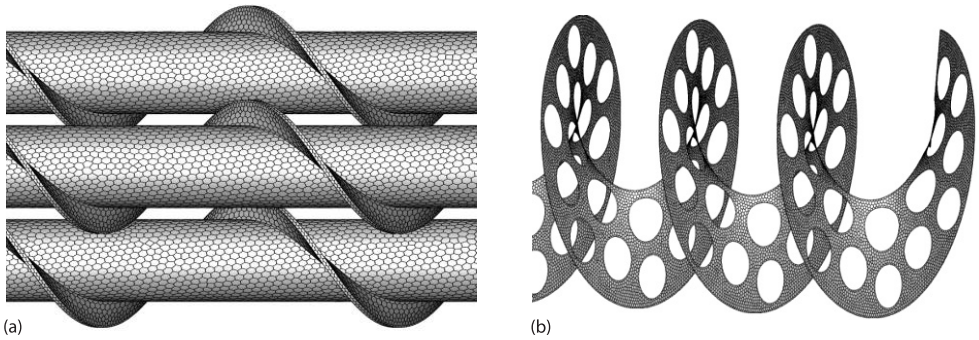

Figure 2. Grid of supporting structure; (a) self-supporting fin tubes and (b) helical baffle

Model checking

It should be noted that STHX-HBST proposed in this study has not been reported in previous study [19, 24]. It is not feasible to validate the results of the numerical simulation based on the existing experimental data. To evaluate the accuracy of the numerical model, model validations were carried out for both the STHX-SG and STHX-HBCT. A small STHX-SG model identical to that in [23] was established, and the simulation results were compared with those obtained by the Bell-Delaware method and the

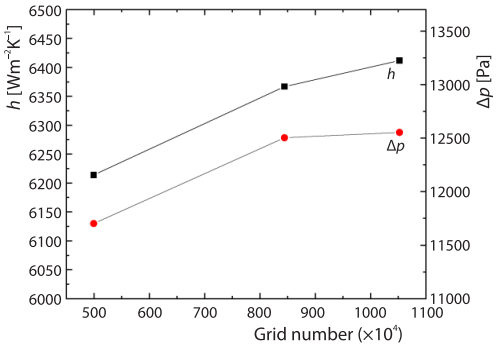

Figure 3. Grid independence test of STHX-HBST

research results of Ozden. As shown in fig. 4, the average errors of heat transfer rate, Q, were 9.38% and 4.7%, respectively, the average errors of the h were 17.12% and 11.1%, respectively. The model of STHX-HBCT in [25, 26] was simulated, as presented in fig. 5, the average errors of the Δp and the h were 21.3% and 19.7%, respectively. Since the leakage flow between the baffles and the heat exchange tubes, the bypass flow between the baffles and the shell, and the heat dissipation process between the heat exchanger and the external environment were not taken into account, the numerical simulation results were higher than both the predictions of the Bell-Delaware method and the experimental measurement values. The computational errors arising from the model simplification were within acceptable range, indicating that the numerical model established in this study is accurate.

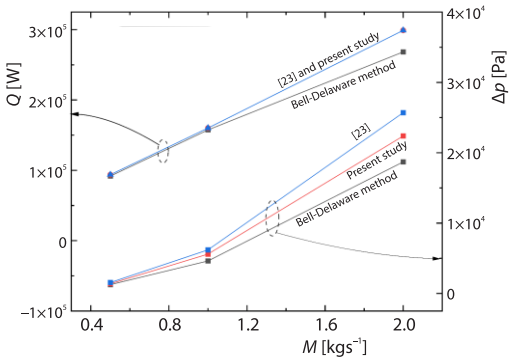

Figure 4. Comparisons of present study and Bell-Delaware method and [23] for STHX-SG

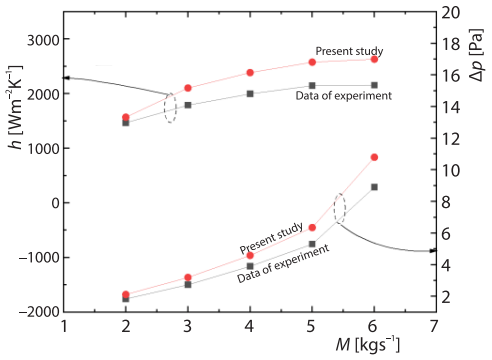

Figure 5. Comparisons of present study with experimental result for STHX-HB

Data reduction

The total heat transfer during the process is:

$$Q = C_p M (T_{\text{out}} - T_{\text{in}}) \tag{7}$$

where T_{out} and T_{in} are the standard outlet and inlet temperatures.

The convective heat transfer coefficient h can be calculated:

$$h = \frac{Q}{A\Delta t_m} \tag{8}$$

where A is the total heat transfer area of the heat exchanger tubes and Δt_m – the logarithmic mean temperature difference, which can be defined:

$$A = N_t \pi \mathrm{d} L \tag{9}$$

$$\Delta t_m = \frac{(T_{\text{w}} - T_{\text{in}}) - (T_{\text{w}} - T_{\text{out}})}{\ln\left[\dfrac{T_{\text{w}} - T_{\text{in}}}{T_{\text{w}} - T_{\text{out}}}\right]} \tag{10}$$

where T_{w} is the tube wall temperature, N_t – heat exchanger tubes number, and L – the effective length of the heat exchanger.

The EEC [27] is used as comprehensive performance indicator for heat exchangers. It characterizes the comparison of the heat transfer obtained per unit energy cost among different devices. Higher EEC value indicates better comprehensive performance of the improved

device. In this paper, the mass-flow rate of the shell side of the heat exchanger is equal, the expression for EEC:

$$EEC = \frac{\frac{Q_{\mathrm{m}}}{Q_{\mathrm{o}}}}{\frac{\Delta p_m}{\Delta p_0}} \tag{11}$$

where the subscripts m and o are the modified and original model, respectively, and Δp_{m} and Δp_{o} – the pressure drops of the respective devices.

Analyses on simulation results

Comparisons among different STHX

The distinct support structures induce significant variations in fluid-flow patterns among different STHX configurations. Figure 6 shows the flow paths generated in four STHX when the mass-flow rate is 2 kg/s. The STHX-SG exhibits zigzag flow pattern with re-circulation zones developing on the leeward side of baffles. In contrast, both STHX-HB and STHX-HBCT configurations show similar flow fields characterized by eliminated flow stagnation zones and enhanced fluid mixing efficiency. The most complex flow dynamics emerge in STHX-HBST, where fluid periodically alternates between composite channels formed by interactions between baffle and fins. Near the peripheral tube bundle, spiral baffle constraints induce helical flow, while central region flow demonstrates spiral movement around individual tubes governed by fin geometry. The flow paths exhibit helical flow characteristics in certain regions, the global flow pattern demonstrates complexity and irregularity under synergistic interactions of two support structures.

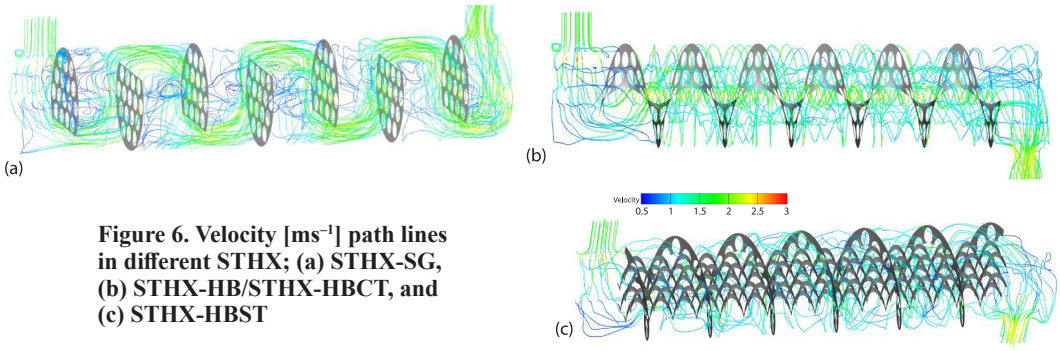

Figure 6. Velocity [ms^{-1}] path lines in different STHX; (a) STHX-SG, (b) STHX-HB/STHX-HBCT, and (c) STHX-HBST

Figure 7 presents the pressure drop characteristics of four STHX under the same mass-flow rate. The pressure drop of all heat exchangers increases significantly with the mass-flow rate increases. The STHX-SG and the STHX-HBCT exhibit the highest pressure drops, with values very close to each other. For STHX-SG, the rapid reduction in flow area at the baffle cut caused significant changes in fluid velocity vectors, leading to momentum losses and sharply increase in pressure drop. For the STHX-HBCT, the reduction in flow area near the central tube leads to significant increase in fluid velocity, which also enhances fluid turbulence intensity. The Δp of STHX-HBCT is higher than that of STHX-HB and almost equal to that of STHX-SG. The STHX-HBST demonstrates the most significant reduction of Δp, reducing by 51.2% and 33.5% compared to STHX-SG and STHX-HB, respectively. This fully demonstrates the superior ability of combined configuration reduce flow resistance, which is crucial

for improving the comprehensive performance of STHX-HBST. Figure 8 illustrates the variation of heat transfer performance among four STHX at various flow rate. The Q and h of the four STHX exhibit similar trends. Within the given mass-flow rate range, the total heat transfer of STHX-HBST is reduced by 12.1%-17.3%, 10.9%-15.3% and 5.8%-11.7% compared to STHX-HBCT, STHX-HB, and STHX-SG, respectively.

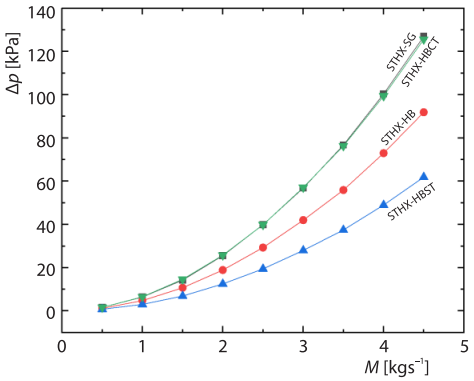

Figure 7. The variation of Δ*p* with mass-flow rate increasing

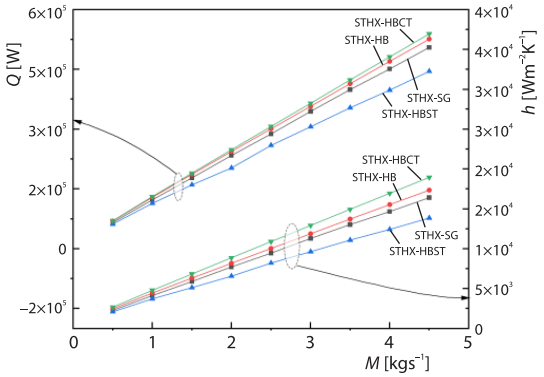

Figure 8. The variation of *Q* and *h* with mass-flow rate increasing

As fig. 9 depicts that the EEC of STHX-HBST, STHX-HB, and STHX-HBCT are all greater than 1, this indicates that the comprehensive heat transfer performance of the three heat exchangers is superior than STHX-SG. The average comprehensive heat transfer performance of STHX-HBST, STHX-HB, and STHX-HBCT improves by 85%, 42%, and 6.1%, respectively compared with STHX-SG. Compared with the reduction in heat transfer, the energy conservation benefits from reduced power consumption outweigh the heat transfer reduction, resulting in higher EEC. The Q per Δp is also an indicator to measure the comprehensive performance of STHX. As shown in fig. 10 the heat transfer growth curves of the four STHX gradually flatten as the Δp increases, the Q obtained by STHX-HBST is higher than that of the other three STHXs at any Δp, which is consistent with the calculation results of EEC. Therefore, it can be considered that comprehensive performance of STHX-HBST is highest among four STHX.

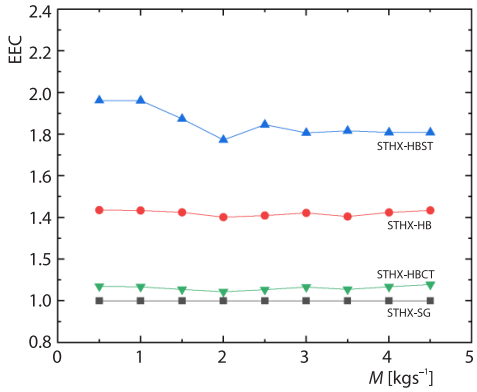

Figure 9. The EEC with various flow rate of four STHX

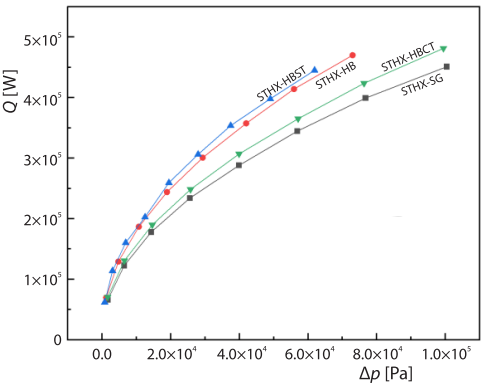

Figure 10. Value of *Q* changes *vs.* Δ*p* for the STHX

The analysis of the fin helix angle

Compared to STHX-HBCT, STHX-HBST uses fins instead of helical baffles in central region of the shell. The fins make point contact with tube walls to provide support, addressing the issues of insufficient utilization of shell side space and degradation of comprehensive performance caused by the installation of central tube. Therefore, investigating the effect of different self-supporting fins helix angle in STHX-HBST is of great significance.

Figure 11 illustrates the trend of local convective heat transfer coefficient across axial cross-sections at an inlet flow rate of 2 kg/s under different fin helix angles. The flow process is divided into three-stages: inlet section, oscillation section, outlet section. For different helix angles, the trends of local h along the axial cross-sections vary significantly in the oscillation section. As the fluid enters the shell from the nozzle, the increase in flow area leads to a reduction in fluid velocity. This decrease in velocity weakens the scouring effect on the tube bundle, causing h to gradually decrease. When the fluid-flows into the complex channels formed by the baffle and fins, the flow passage cross-sectional area alternately contracts and expands in a regular pattern, leading to an approximately periodic oscillation trend in local h. Additionally, larger helix angle results in greater fin pitch, increasing the oscillation period. As fluid-flows through the outlet pipe, the reduction of flow area increases fluid velocity, enhancing turbulence and causing an increase in h. However, the axial h decreases with increasing helix angle due to the enlarged flow area reducing fluid disturbance to the boundary-layer, thereby lowering heat transfer efficiency. As shown in the fig. 12, to further investigate the distribution of the h across tubes in different layers, the tubes are designated as Tubes 1-3 based on radial distance. Figure 13 illustrates the variation in h of tubes with helix angle at inlet mass-flow rate of 2 kg/s. The surface h of the three tubes decreases as the helix angle increases. Within

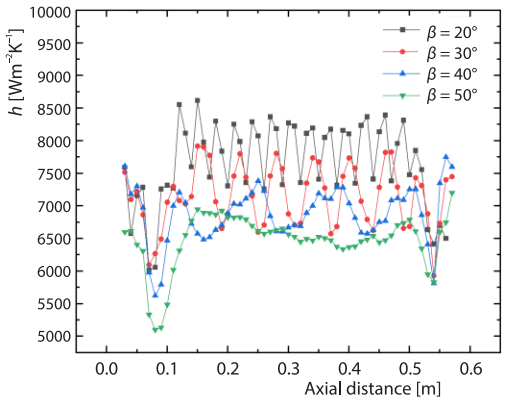

Figure 11. Distribution of the average surface h along the shell-side axis under different helix angles

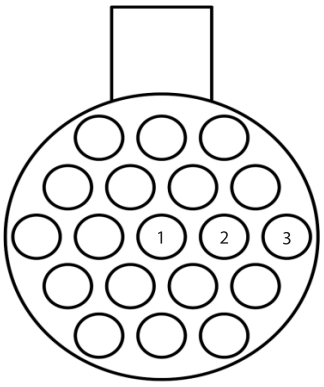

Figure 12. Distribution of heat exchange tubes at different radial distances

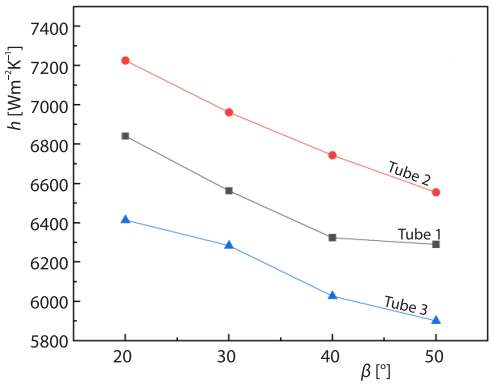

Figure 13. The h of tubes under different helix angles

the studied flow rate range, their surface h values exhibit reductions of 8.1%, 9.2%, and 7.9%, respectively. The h of tubes decreases as the radial distance increases and because the self-supporting fins exhibit smaller pitch dimensions compared to helical baffles, higher fluid velocity prevails around inner tubes relative to outer tube bundles, generating enhanced scouring effects that disrupt thermal boundary-layers.

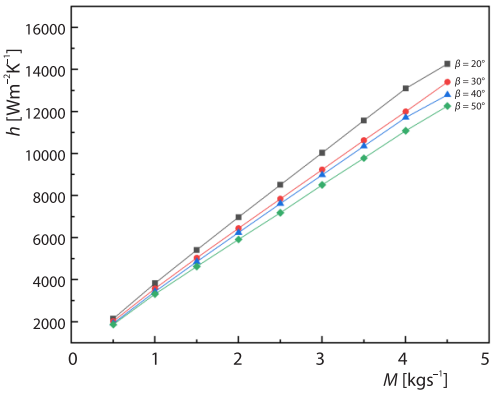

Figure 14. Variation of h with mass-flow rate increase at different helix angles

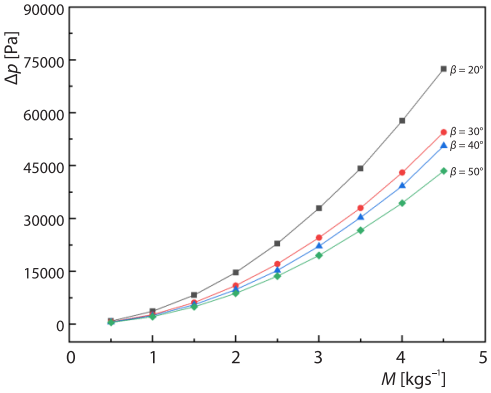

Figure 15. The variation of Δp with mass-flow rate increase at different helix angles

Figures 14 and 15 illustrate the variations of h and Δp with mass-flow rate under different helix angles. Both the h and Δp decrease as the helix angle increases, as the increase in fin pitch leads to an increase in the axial velocity component of the fluid near the finned tubes while reducing the rotational velocity component in the shell cross-section. The flow pattern gradually shifts towards longitudinal flow, weakening the shear effect on the thermal boundary-layer. The comprehensive performance, $h/\Delta p$, under different fin helix angles is shown in fig. 16. It sharply decreases in low Reynolds number region. As the mass-flow rate increases, this downward trend gradually becomes less steep. At the same mass-flow rate, the $h/\Delta p$ goes up with the increase of the helix angle. Compared to the 20° helix angle, the 50° helix angle shows improvement in comprehensive performance ranging from 40.21% to 47.71%.

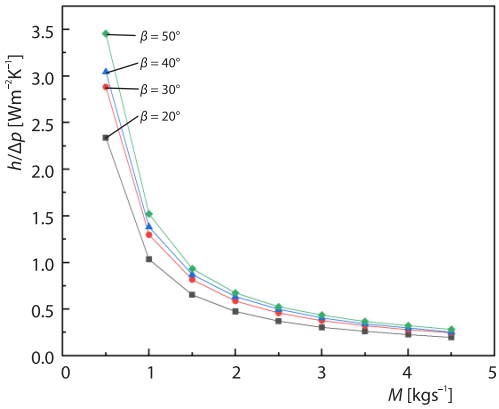

Figure 16. The variation of $h/\Delta p$ with mass-flow rate for different helix angles

Conclusions

In this paper, a novel heat exchanger named STHX-HBST was proposed. Numerical simulation of four STHX with different configurations was conducted, the effects of the fin helix angle on the flow and heat transfer performance of STHX-HBST were analyzed. The conclusions are as follows.

- The EEC of STHX-HBST increases by 85%, 74.3%, and 30.2% compared with STHX-SG, STHX-HBCT, and STHX-HB, respectively. The total heat transfer under the same pressure drop is highest among four STHX, the benefits of reduced power consumption outweigh the reduction in heat transfer.

- The local h on the axial cross-section of STHX-HBST exhibits approximately periodic variation and decreases with increase of fin helix angle. As the fin helix angle grows, both the h and Δp of STHX-HBST show decreasing trend, while the trend of comprehensive performance is opposite. Compared to helix angle of 20°, the comprehensive performance, $h/\Delta p$, at helix angle of 50° improves by 40.21%-47.71%.

References

[1] Nazari, M. A., *et al*., Intelligent Techniques for Prediction Characteristics of Shell and Tube Heat Exchangers: A Comprehensive Review, *International Communications in Heat and Mass Transfer*, *158* (2024), 107864
[2] Mohammadzadeh, A. M., *et al*., Comprehensive Numerical Investigation of the Effect of Various Baffle Design and Baffle Spacing on a Shell and Tube Heat Exchanger, *Applied Thermal Engineering*, *249* (2024), 123305
[3] Lutcha, J., Nemcansky, J., Performance Improvement of Tubular Heat Exchangers by Helical Baffles, *Chemical Engineering Research and Design*, *68* (1990), 3, pp. 263-270
[4] Wang, Q., *et al*., Experimental Study and Genetic-Algorithm-Based Correlation on Shell-Side Heat Transfer and Flow Performance of Three Different Types of Shell-and-Tube Heat Exchangers, *ASME. J. Heat Transfer*, *129* (2007), 9, pp. 1277-1285
[5] El Maakoul, A., *et al*., Numerical Comparison of Shell-Side Performance for Shell and Tube Heat Exchangers with Trefoil-Hole, Helical and Segmental Baffles, *Applied Thermal Engineering*, *109* (2016), Part A, pp. 175-185
[6] Hamied, M. A., *et al*., A Novel Sequential Approach through Structural Enhancements for Designing a New Serrated Helical Heat Exchanger, *Case Studies in Thermal Engineering*, *699* (2025), 106006
[7] Mohammadzadeh, A. M., *et al*., Comprehensive Numerical Investigation of the Effect of Various Baffle Design and Baffle Spacing on a Shell and Tube Heat Exchanger, *Applied Thermal Engineering*, *249* (2024), 123305
[8] Zhang, M., *et al*., The CFD Simulation on Shell-and-Tube Heat Exchangers with Small-Angle Helical Baffles, *Frontiers of Chemical Science and Engineering*, *9* (2015), 2, pp. 183-193
[9] Lei, Y. G., *et al*., Effects of Baffle Inclination Angle on Flow and Heat Transfer of a Heat Exchanger with Helical Baffles, *Chemical Engineering and Processing: Process Intensification*, *47* (2008), 12, pp. 2336-2345
[10] Xiao, X., *et al*., Numerical Investigation of Helical Baffles Heat Exchanger with Different Prandtl Number Fluids, *International Journal of Heat and Mass Transfer*, *63* (2013), Aug., pp. 434-444
[11] Dong, C., *et al*., Influence of Baffle Configurations on Flow and Heat Transfer Characteristics of Trisection Helical Baffle Heat Exchangers, *Energy Conversion And Management*, *88* (2014), Dec., pp. 251-258
[12] Du, W., *et al*., Evaluation of Shell Side Performance and Analysis on Continuous Helical Baffled Heat Exchangers with Elliptical Tubes, *Journal of Chemical Industry and Engineering*, *64* (2013), 4, pp. 1145-1150
[13] Zhang, Z., *et al*., An Experimental Heat Transfer Study for Helically Flowing Outside Petal-Shaped Finned Tubes with Different Geometrical Parameters, *Applied Thermal Engineering*, *27* (2007), 1, pp. 268-272
[14] Gu, X., *et al*., Heat Transfer and Flow Resistance Characteristics of Helical Baffle Heat Exchangers with Twisted Oval Tube, *Journal of Thermal Science*, *31* (2022), 2, pp. 370-378
[15] Wang, S., *et al*., Experimental Investigation on Heat Transfer Enhancement of a Heat Exchanger with Helical Baffles through Blockage of Triangle Leakage Zones, *Applied Thermal Engineering*, *67* (2014), 1-2, pp. 122-130
[16] Zhang, J. F., *et al*., The 3-D Numerical Simulation on Shell-and-Tube Heat Exchangers with Middle-Overlapped Helical Baffles and Continuous Baffles – Part II: Simulation Results of Periodic Model and Comparison between Continuous and non-Continuous Helical Baffles, *International Journal of Heat and Mass Transfer*, *52* (2009), 23-24, pp. 5381-5389
[17] Wang, Q., *et al*., Review of Improvements on Shell-and-Tube Heat Exchangers with Helical Baffles, *Heat Transfer Engineering*, *31* (2010), 10, pp. 836-853
[18] Wang, Q., *et al*., Numerical Investigation on Combined Multiple Shell-Pass Shell-and-Tube Heat Exchanger with Continuous Helical Baffles, *International Journal of Heat and Mass Transfer*, *52* (2009), 5-6, pp. 1214-1222

[19] Yang, J. F., *et al*., Numerical Investigation on Combined Single Shell-Pass Shell-and-Tube Heat Exchanger with Two-Layer Continuous Helical Baffles, *International Journal of Heat and Mass Transfer*, *84* (2015), May, pp. 103-113
[20] Uosofvand, H., *et al*., Shell-and-Tube Heat Exchangers Performance Improvement Employing Hybrid Segmental – Helical Baffles and Ribbed Tubes Combination, *Journal of the Brazilian Society of Mechanical Sciences and Engineering*, *43* (2021), 8, pp. 1-15
[21] Wu, J. X, *et al*., Numerical Analysis and Experiment on Heat Transfer Enhancement of the Helical Ribbed Heat Exchanger, *Engineering Thermophysics*, *29* (2008), 5, pp. 861-864
[22] Lei, Y. G., *et al*., Design and Optimization of Heat Exchangers with Helical Baffles, *Chemical Engineering Science*, *63* (2008), 17, pp. 4386-4395
[23] Ozden, E., Tari, I., Shell Side CFD Analysis of a Small Shell-and-Tube Heat Exchanger, *Energy Conversion and Management*, *51* (2010), 5, pp. 1004-1014
[24] Abbasian Arani, A. A., Uosofvand, H., Improving Shell and Tube Heat Exchanger Thermohydraulic Performance Using Combined Baffle, *International Journal of Numerical Methods for Heat & Fluid-Flo*w, *30* (2020), 8, pp. 4119-4140
[25] Cao, X., *et al*., Numerical Investigation and Experimental Validation of Thermo-Hydraulic and Thermodynamic Performances of Helical Baffle Heat Exchangers with Different Baffle Configurations, *International Journal of Heat and Mass Transfer*, *160* (2020), 120181
[26] Shui, J., Mechanism Analysis and Performance Study of Flow and Heat Transfer in Shell-Side of Shell-and-Tube Heat Exchanger with Helical Baffles, Ph. D. thesis, Shandong University, Shandong, China, 2011
[27] Liu, W., *et al*., Application of a Multi-Field Synergy Principle in the Performance Evaluation of Convective Heat Transfer Enhancement in a Tube, *Chinese Science Bulletin*, *57* (2012), 10, pp. 867-874

Paper submitted: March 21, 2025
Paper revised: May 25, 2025
Paper accepted: May 30, 2025